AIAA 2002-3156

Active Control of Separation from the Slat Shoulder of a Supercritical Airfoil

L. G. Pack, N. W. Schaeffler and C. S. Yao
NASA Langley Research Center
Hampton, VA

A. Seifert
Tel-Aviv University, Ramat-Aviv, Israel
and
ICASE, NASA Langley Research Center
Hampton, VA

1st Flow Control Conference
24–26 June 2002
St. Louis, Missouri

Active Control of Flow Separation from the Slat Shoulder of a Supercritical Airfoil

LaTunia G. Pack*, Norman W. Schaeffler†, Chung-Sheng Yao‡
Flow Physics and Control Branch
NASA Langley Research Center, Hampton, VA 23681
and

Avi Seifert§
Tel-Aviv University, Ramat-Aviv 69978, ISRAEL and ICASE, Hampton, VA 23681

Abstract

Active flow control in the form of periodic zero-mass-flux excitation was applied at the slat shoulder of a simplified high-lift airfoil to delay flow separation. The NASA Energy Efficient Transport (EET) supercritical airfoil was equipped with a 15% chord simply hinged leading edge slat and a 25% chord simply hinged trailing edge flap. The cruise configuration data was successfully reproduced, repeating previous experiments. The effects of flap and slat deflection angles on the performance of the airfoil integral parameters were quantified. Detailed flow features were measured as well, in an attempt to identify optimal actuator placement. The measurements included, steady and unsteady model and tunnel wall pressures, wake surveys, arrays of surface hot-films, flow visualization and Particle Image Velocimetry (PIV). High frequency periodic excitation was applied to delay the occurrence of slat stall and improve the maximum lift by 10 to 15%. Low frequency amplitude modulation was used to reduce the oscillatory momentum coefficient by roughly 50% with similar aerodynamic performance.

Nomenclature

AFC Active Flow Control
AM Amplitude Modulation
α Angle of Attack
c_μ steady blowing momentum coefficient , $\equiv J/cq$
$\langle c_\mu \rangle$ oscillatory blowing momentum coefficient, $\equiv < J' > /cq$
C_μ combined blowing momentum coefficient, $\equiv \left(c_\mu ; < c_\mu > \right)$
c model chord
C_{dp} pressure drag coefficient
C_L lift coefficient
$C_{L,max}$ maximum lift coefficient
C_p wall pressure coefficient, $\equiv (P - P_S)/q$
$C_{p,min}$ minimum pressure coefficient
δ_f flap deflection
δ_s slat deflection
f oscillation frequency [Hz]
F^+ reduced frequency, $\equiv (f\, x_{sp})/U_\infty$
h slot height or width
J momentum at slot exit, $\equiv \rho h U_j^2$
M Mach number
P pressure

* Member AIAA, l.g.pack@larc.nasa.gov
† Member AIAA, n.w.schaeffler@larc.nasa.gov
‡ c.s.yao@larc.nasa.gov
§ Associate Fellow, AIAA, seifert@eng.tau.ac.il

q freestream dynamic pressure, $\equiv 1/2\rho U_\infty^2$

R_c chord Reynolds number, $\equiv U_\infty c/\nu$

T temperature

U, u average and fluctuating streamwise velocity

x/c normalized streamwise location

X_{sp} distance from baseline separation to reattachment

z spanwise location

ν kinematic viscosity

ρ density

Abbreviations

LE leading edge

TE trailing edge

< > phase locked values

Subscripts

b baseline flow conditions

c cavity

d de-rectified hot-wire data

j conditions at blowing slot

N Normalized according to text

R reattachment

S separation

∞ free-stream conditions

2D two-dimensional

3D three-dimensional

Superscripts

′ root mean square of fluctuating value

Introduction

Following successful demonstration of active separation control using oscillatory flow excitation at flight Reynolds numbers[1,2] and taking into consideration an industry system study[3] indicating the possibility of significant payoffs such as cost, weight and drag reductions, it was decided to apply active separation control to a simplified high-lift system. The purpose of the current investigation is to explore ways to simplify current multi-element high-lift airfoils[4] that use slots and the Fowler effect to generate high-lift. The chosen design completely eliminates hinges and positioning actuators that are external to the airfoil contour as well as slots for energizing the boundary layer. All hinges are internal as will be the positioning actuators, thus reducing parasite drag at cruise. The danger of laminar leading edge (LE) separation is eliminated by the use of a simply hinged LE slat. Zero-mass-flux periodic excitation is applied at locations that are prone to separation, i.e. the slat and flap shoulders.

The Experiment

The Wind Tunnel

The test was conducted in the Basic Aerodynamic Research Tunnel (BART) located at NASA Langley Research Center. The BART facility is a low speed open-circuit wind tunnel with a 0.71 m high by 1.02 m wide by 3.05 m long test section. The maximum speed of the tunnel is approximately 60 m/s (Re/m=0.345x10^6). The wind tunnel is used primarily as a flow physics facility; therefore, it has the instrumentation and optical access needed for measurement techniques such as LDV and PIV.

Simplified High-Lift Model

The simplified high lift version of the NASA EET model[4] was designed in a modular manner so that zero-net mass flux actuators could replace solid regions in the model near the slat and flap shoulders (Figs. 1a and 1b). This paper will focus on results obtained when introducing periodic excitation near the slat shoulder. The 406.4mm chord model has a 15% chord leading edge slat that can be deflected from 0 to -30 deg and a 25% chord trailing edge flap that can be deflected from 0 to 60 deg. Figure 2 shows a picture of the model installed in the wind tunnel with the flap and slat deflected. Angle of attack settings for the airfoil, the flap, and the slat were all automated and computer controlled. The model has 78 streamwise static pressure taps located at mid span and 2 rows of 18 spanwise static pressure taps spaced 50.8mm apart located at x/c=0.35 and x/c=0.94. In addition to the static pressure taps, there are nine unsteady pressure transducers on the model surface (Fig. 1b) and two unsteady pressure transducers embedded in the leading edge (slat) actuator cavity for monitoring the pressure fluctuations produced by the actuator and correlating the wind tunnel experiment with the bench-top actuator calibration tests.

A wake-rake was located 4.6 chords downstream of the model mid chord. The wake rake was comprised of 31 total pressure probes with a 17.8mm spacing between each probe and was mounted on a traverse system to allow any desired resolution of wake data. Pressure belts were placed on the floor and ceiling (when glass ceiling in place) of the tunnel to gather wall pressure data that would be used for wind tunnel wall interference correction. The data presented in this paper has not been corrected for wind tunnel wall interference using the wall pressure signature method.

Hot-film Arrays

To aid in determining the locations of transition and separation, 48 hot-films were installed on the model. On each element (slat, flap, and main) of the model there are 16 hot-film sensors approximately 50.8mm to the right of the model centerline (and therefore from the steady pressure tap locations) (Fig. 1b). A 16-channel constant temperature anemometer coupled with a switch matrix was used to operate and acquire data from the 48 hot-films on the model. The hot-

films on each element of the model were acquired simultaneously using a 16 bit high speed analog-to-digital converter. The data were low pass filtered at 10KHz and sampled at 25.6 KHz. The films were operated at an overheat ratio of 1.2. Each anemometer channel had 3 films that could be assigned to it through the switch matrix. Tuning was optimized for the set of three films. The hot-film sensors were 0.4mm long. The films were etched onto a polyimide sheet and then bonded to the model. The polyimide sheet covered one half of the span of the model. A small step (0.1mm) exists at the juncture between the polyimide sheet and the model and body filler was used to smooth/fair the step.

Slat Actuator

An internal piezo-electric actuator was placed at the slat shoulder. The actuator had two slots located at x/c=0.14 and x/c=0.3. The slots were inclined approximately 30^o to the surface, facing downstream and were 0.88 and 0.5 mm wide respectively. The forward slot could have been hidden under the slat at stowed condition to eliminate possible detrimental effects of an exposed slot at cruise, if a slat with a sharper trailing edge had been fabricated. The x/c=0.3 slot had an alternative cover plate for sealing the slot. A comprehensive bench-top calibration was performed on the LE actuator prior to installation in the tunnel and unsteady pressure transducers were installed in the actuator's cavity to monitor its operation while in the tunnel. The LE actuator was operated at its resonance frequency (853±5 Hz or 1±0.005KHz depending on the type of Piezo elements installed) using a pure sine wave and also with an amplitude modulation (AM) at an order of magnitude lower than the resonance frequency.

Flow Visualization

A commercially available smoke generator was used to seed the flow with smoke for the flow visualization study performed. The smoke was introduced upstream of the contraction and still as well as video photography were used to acquire the images. An argon ion laser was used to improve the flow visualization quality.

PIV Set-Up

Digital PIV was used to measure the instantaneous flow fields phase synchronized with the leading edge actuator cycle. The PIV system includes two 1Kx1K cameras installed side by side with 105mm Macro lens. The field of view from each camera was overlapped to cover both leading edge actuator slot locations above the airfoil. The magnification of the imaging system was about 9:1 with the measurement plane about 70mm wide. Each interrogation area at the grid point has 24x24 pixel resolution and this corresponds to about 1.5 mm square at the measurement plane. Maximum 50% overlap between adjacent interrogation regions was used. Smoke, introduced upstream of the contraction, was used for seeding. Dual Nd-Yag lasers were used to illuminate a light sheet, placed about 50mm off the model centerline. The laser pulse separation was set at 6-8 microsecond to cover a free stream velocity of about 30 m/sec. Ensemble averages at up to eight phases from about 100 data sets in each phase were computed. Phase averaged mean field and perturbation fields from the phase mean were also estimated.

Experimental Uncertainty

The α's presented are accurate to within ±0.03^o. The slat and flap deflection angles are accurate to within ±0.25^o, $<c_\mu>$ is accurate to within 20%, R_c is accurate to within 3%, and the slot width is accurate to within ±0.08mm.

The uncertainty of the airfoil integral parameters are listed in the Table 1 (in absolute values and related to flow conditions)

Parameter	Fully attached	Stalled	Controlled
C_L	.01	0.04	.02
C_{dp}	.002	.004	.003
C_D	.002	.008	.006

Table 1: Uncertainty of Airfoil integral parameters.

The large uncertainty in the total drag, C_D is due to the extrapolation of the wake data for some of the high lift configurations of the airfoil.

3 Discussion of Results

3.1 Baseline

The baseline cruise configuration of the airfoil was tested and compared to previous tests of the same airfoil at a different facility and a different range of Mach and Reynolds numbers[4]. This data was acquired with the original airfoil contour, before any actuator slots were present. The lighter color regions shown in Figure 1a indicate alternative actuator locations. The highest available R_c at BART, $1.5x10^6$, is lower than the lowest R_c tested in the LTPT, $2.5x10^6$. Figure 3a presents the lift data of the current vs. the data from Lin[5]. The lift data indicate that, as expected, significant wall interference exists in the present BART set-up. Conventional wind tunnel walls interference and wake blockage corrections[6] were applied to the data and the corrected BART lift (for

R_c=1.5x10^6) is in very good agreement with the LTPT data (for R_c=2.5x10^6) for the cruise configuration. Weak R_c effects such as increased lift at low α (due to a laminar separation bubble as shown in Fig. 3b) and earlier stall (due to a thicker BL) can be seen. But overall the reproduction of the LTPT data is satisfactory. Uncorrected lift data measured at BART at R_c=0.75x10^6 is also shown for comparison and is in good agreement with the higher R_c data from LTPT and the corrected BART data for R_c=1.5x10^6. Besides stronger R_c effects (shown for instance in the Cp of Fig. 3b), the three data sets are in reasonable agreement. Most of the data to be presented in this manuscript is for R_c=0.75x10^6 and attention is paid that turbulent separation would always be considered, minimizing low R_c effects.

It is expected that wall interference will have a larger influence on the flow as the lift and drag increase, due to slat and flap deflections for the high lift configuration. However, the lift increment and especially the drag reduction with active separation control are expected to be conservative since tunnel interference, at least the wake blockage effect of it, will be reduced since the drag will decrease. Moreover, floor and ceiling pressures were acquired at all flow conditions, to assist future data reduction and comparison to CFD, taking into account the tunnel walls.

The baseline high-lift characteristics of the simplified high lift system will now be presented and discussed, including the effect of opening 2D actuator slots in the airfoil upper surface. The purpose of deflecting the LE slat was to eliminate the possibility of LE separation that supercritical airfoils are notoriously known for due to the low radius of curvature of the LE[7].

Figure 4 demonstrates the effect of deflecting the slat on the lifting performance of the baseline airfoil at a fixed flap deflection angle of 0^o. The main effect of the slat deflection is to delay stall to a larger incidence and therefore increase the maximum lift generated by the airfoil. The stall is also milder at larger slat deflections, alleviating the abrupt stall shown for zero slat deflection. A secondary effect is a somewhat lower lift at low incidence and increased $d(C_L)/d(\alpha)$ in agreement with the progressively more chambered airfoil. The –30^o slat deflection data is considered an anomaly, as stall was not encountered in the available range of α's, presumably due to tunnel interference, and therefore will not be considered. Overall, the slat has little effect on the pre-stall lifting performance of the airfoil.

Even though the main focus of this paper is on actuation provided at the slat shoulder to delay BL separation downstream of the slat, in application it will be required to consider both slat and flap deflections for typical landing and to a lower extent for take-off. Figure 5a shows the lift data for increasing flap deflection at R_c=0.75x10^6. The typical flap effect[8] is shown where the lift is increased over the entire α range as the flap is deflected. Figure 5b presents the lift vs. form drag data, showing the flap effect as well. From the lift vs. form drag data it is evident that the flapped airfoil behaves as a chambered airfoil up to a flap deflection between 10^o and 15^o, where the lift slope decreases with the incidence due to developing TE separation (5a). At a flap deflection angle of 15^o, the flap upper surface is separated from the flap shoulder, causing a significant drag increase (5b) and a constant lift slope (5a) prior to stall that occurs at progressively smaller incidence as the flap deflection angle increases (5a). This abrupt lift reduction occurs because separation abruptly shifts from the flap shoulder to the LE.
Fig. 5c shows the maximum lift of the flapped airfoil at zero slat deflection and compares it to the corrected maximum lift according to Reference 6, taking the form-drag for the wake blockage corrections, as it is not practical to measure wake drag at these highly unsteady separated flow conditions. The corrected flapped airfoil lift data shows that significant tunnel interference exists, and as expected, the value of $d(C_L)/d(\delta_f)$ decreases significantly for δ_f>7.5^o. Negligible lift increments are obtained for flap deflections larger that 35^o. However, this could be altered if high frequency periodic excitation would be provided at the flap shoulder to increase the suction level there.

A candidate flow condition (δ_s=-25^o and δ_f=30^o) for a landing configuration is shown in Fig. 6. The data presented in this figure includes the cruise configuration, slat deflection of -25^o at zero flap deflection (showing delayed and milder stall), flap deflection of 30^o at zero slat deflection (showing increased lift and earlier, more abrupt stall), and a combination of slat deflection of -25^o and flap deflection of 30^o. The lift data for the latter configuration shows that the slat effect is almost linearly added to the flap effect and its stall "milding" capability is maintained even at a flap deflection of 30^o. The challenge is now to apply periodic excitation on both the slat and flap shoulders, delay BL separation at both locations allowing larger flap and slat deflections with a resulting enhanced lift.

In what follows we shall discuss the effects of machining slots in the airfoil contour, studying its

effect on the baseline airfoil performance and thereafter applying periodic excitation at the slat shoulder. Future publications will present results for flap excitation and combinations of the two.

Well-optimized airfoils at relevant Reynolds numbers might suffer performance losses due to the addition of surface discontinuities. These could take the form of the actuator slots. When AFC is considered for performance improvement, one should carefully consider the associated losses due to the mere presence of a slot. If performance losses are deemed too large, care should be taken to seal or hide the slots in the cruise stowed configuration.

Fig. 7 presents the effect of introducing a total of six slots, two slots at the slat shoulder (i.e. at x/c=0.14 and x/c=0.3) and 3 sealed and one open slot on the flap, on the pressure distribution and lift performance of the airfoil for a high-lift configuration. The data shows that up to $C_{L,max}$ (i.e. 13°) there is no measurable effect on C_p or C_L of the airfoil. The flap slots are not considered important at this flap deflection as separation takes place at the flap shoulder (i.e. perhaps only the most upstream flap slot is in an attached flow region) Only the post stall performance is affected in a measurable manner, due to the slat actuator slots, especially the stalling slope. The sensitivity of the pressure distribution at post stall conditions to the slots on the slat actuator indicates that the slat actuator slots were machined in the right location to delay stall in the above configuration.

The effect of slat separation control was initially studied with a small flap deflection in order to allow reattachment to the entire airfoil upper contour with effective slat control and eliminate adverse effects due to unsteady interaction with the massively separated flap region flow present at large flap deflections.

Figure 8 shows the effect of the slat deflection angle on the maximum lift coefficient of the airfoil at a fixed low flap deflection, for the baseline (with slots, no AFC) and the optimally controlled airfoil by high frequency excitation. Figure 9 presents baseline and controlled C_l-α curves, showing that a milder stall is gradually generated with a moderate increase in $C_{l,\max}$. For slat deflections below –10°, the laminar flow separates at the LE and therefore the activation of the slat actuator (located at x/c=0.14) is not effective. Once separation at high α's is shifted to the slat shoulder, the actuators delays stall by 1-2 deg and increase the maximum obtainable lift (Figs. 8-9). Optimum performance is achieved at a slat deflection of -25°. The actuator was operated near resonance, f=853Hz, for the above data set, resulting in a F^+=10.5 (length scale is distance from forward slat actuator slot to trailing edge). However it will later be shown that by using amplitude modulation of the high frequency excitation by F^+ order unity, one can obtain the same aerodynamic performance at half the momentum input.

From this point, the paper will concentrate on physical description of the baseline and controlled flows close to maximum lift condition, i.e. slat deflection of -25°, flap deflection of 30° and α of 15°. This flow condition was selected as it closely represents a high-lift landing configuration that will eventually include also flap shoulder separation control.

Baseline and controlled pressure distributions are presented in Fig. 10a. The baseline flow separates downstream of the slat shoulder at x/c≈0.2, based on the plateau of the pressure distribution. With AFC activated at x/c=0.14 slot, the flow reattaches to the main element and separates only at the flap shoulder. Note that the excitation with an amplitude modulated (AM) signal generates almost the same pressure distribution even though the $<c_\mu>$ was reduced by almost 50% due to the modulation (the peak slot exit velocity is the same). Fig. 10a also shows that using a pure sine wave excitation, with the same momentum coefficient as that of the AM signal, is significantly inferior. The wake surveys for the flow conditions of figure 10a are presented in Figure 10b. They indicate that with control the total drag is reduced very effectively, in agreement with the delayed separation on the airfoil.

The effect of the AM frequency was tested at the same flow condition but with a slightly different airfoil geometry (δ_f=5° instead of δ_f=30°) and the lift and form-drag variations due to the AM frequency are presented in Fig. 11. The $<c_\mu>$ for these data is 0.003%. Note that the lift increment and form-drag reduction are optimally achieved at reduced frequencies in the range 0.25 to 1.25. This is in good agreement with previous work using flow instability for separation control[9,10,11] and excitation of a free jet[12], even though the low frequency excitation is strictly not present in the spectra of the actuator output. However, surface hot-film data indicate that further downstream of the actuator, the sidebands due to the AM (at $f_{res}\pm f_{am}$) develop non-linearly into clear peak at f_{am}. Note that the pure sine wave excitation generates F^+=12.2. This finding indicates the existence of a non-linear mechanism transforming the AM spectra and generating the low frequency motion.

The data clearly shows that excitation at an AM frequency that generates F^+ of order unity, is very effective for separation control at the slat shoulder. Margalit, et. al[13] found that the separated shear layer on a Delta wing was extremely receptive to $F^+O[1]$ AM signal and completely insensitive to the high frequency excitation (F^+ from 20 to 100). Figure 12 shows a comparison of the lift dependence on $<c_\mu>$ for the pure sine and AM excitation signals. The data clearly shows that the $dC_L/d<c_\mu>$ slope for the AM is about twice that of the pure sine wave excitation, resulting in about a 50% reduction in the required $<c_\mu>$ for the same lift increment.

Figure 13a present flow visualization pictures taken at (baseline) post-stall conditions. The upper edge of the baseline smoke plume does not follow the airfoil contour downstream of the slat shoulder, indicative of flow separation. With the application of periodic excitation from the slat shoulder, either with a pure sine wave (Fig. 13b) or with a modulated sine wave (Fig. 13c), the flow reattaches. The reason for the flow reattachment is the generation of convectively unstable vortical structures that are not seen in the flow visualization images but were measured by PIV and also by the hot-films downstream of the excitation slot.

Baseline and phase-locked controlled PIV data taken at the slat shoulder region demonstrate the significant change in the boundary layer vorticity when the excitation was activated and also reveals the generation of coherent structures downstream of the excitation slots, even when using a pure sine wave (e.g. $F^+ \cong 12$). Fig 14a shows constant vorticity contours of the baseline flow while Fig. 14b shows the same type of data for the controlled flow, with the AM signal. The data from the two cameras used for the PIV overlap at x/c=0.21. The coordinates shown in Figures 14 are rotated 15^o, therefore the slat actuator slot at x/c=0.14 is at x/c=0.163. Good agreement was found between the baseline PIV, Cp, and hot-films data indicating that the baseline flow separates at $x/c \cong$ 0.18 to 0.2. When periodic excitation was introduced (this time) only from the x/c=0.14 slot, a healthy attached BL is restored (Fig. 14b) and convectively unstable waves are seen to propagate downstream with an initial wave length of 5%c that increases as it progresses downstream (Fig. 14c, showing the phase–locked vertical component of velocity with a coherent downwards directed momentum transferring velocity) in agreement with Seifert et al[9] and Pack and Seifert[10].

Transition on the slat was detected using the hot-film information[14,15]. It is well established that laminar-turbulent transition is an intermittent process in which turbulent spots appear sporadically in time and from a rather narrow region in space. The spots are associated with high frequency content, and a local alternation of the velocity profile from laminar to turbulent and vise versa (with a calming region following every spot)[16]. The end-result of all these complex physical phenomena can be measured by a significant change in a single quantity, the hot-film RMS. Figure 15 presents the standard deviation of the hot-film voltages wrapped around the leading edge. The stagnation point is marked by a slight increase in RMS associated with the migration of the stagnation point in space due to the flap separated flow and vortex shedding changing the circulation around the entire airfoil. The cross correlation of adjacent sensors around the stagnation point indicates (as noted before by others[14,15]) the presence of a phase reversal due to the opposite wave propagation direction on the two sides of the stagnation point. Transition is evident from the large RMS peak observed on the upper surface. The resolution of the hot-film in space did not always allow capturing this peak, that is a rather local phenomenon. Once transition occurred, the RMS settles to a constant value, about 2 times the laminar RMS in agreement with Betelrud[14].

While transition detection on this model could be determined by considering both the pressure distribution and hot-film RMS values, separation detection proved to be more complex. Nakayama et al.[15] suggests negative correlation coefficient between two consecutive hot-film sensors as a criteria. This criteria assumes that there is a region in the separated flow that on the mean is characterized by a reverse flow, where there will be enough wavy motion moving upstream in the separated region to cause the cross correlation coefficient between two sensors (one upstream and the other downstream of the mean separation region) to be negative. This criterion was attempted presently and failed. Neither visual observation of many events nor detailed calculations provided evidence for the existence of such a physical phenomena leading to a working criteria.

A physical phenomena associated with separation of turbulent boundary layer was sought. It was deemed reasonable to search for a significant change in a surface property that could be directly linked to separation. When one thinks about the distribution and balance between different scales in an attached turbulent BL, and how it would be affected by the occurrence of TBL separation, one would tend to think that a measurable effect should be the disappearance of the smallest turbulent scales from the wall proximity, translated into an intermittent

disappearance of the highest frequency content from the hot-film signal, closest to and downstream of the mean separation location. The intermittent nature of incipient TBL separation eliminates the option of using a long time averaged FFT as a candidate criteria, exactly as it is meaningless to consider the same feature for a transitioning BL. The unsteadiness of the separation location should be enhanced by periodic excitation, especially at $F^+ \cong 1$. Short Time Fourier Transform (STFT) was applied to examine the above idea and develop a separation criteria based on the above consideration. Fig 16 shows long time power spectra of six x/c stations corresponding to the baseline C_p shown in Figure 10a. A distinct change in the FTT could be observed. Contour plots of the STFT are provided for the same data in Figures 17(a)-17(f) with the ordinate being the frequency, the abscissa the mean time of each 40ms window and the colors are the power level in log scale.

It was expected that columns of blue penetrating into the red-yellow regions intermittently, indicating the loss of high frequency content would characterize incipient separation. The baseline data clearly shows this pattern around x/c=0.18, in good agreement with the location of $C_p''=0$ and slightly upstream of the $dC_p/d(x/c)=0$ area on the airfoil. The test of such a criteria is to apply it to several very different flow fields, and later translate it into a simple and numerically efficient criterion. Figures 17(g)-17(x) show the STFT contours for the three other flow conditions shown in Fig 10a. Similar patterns showing the low power at high frequency penetrating into the low frequency region could be shown at $x/c \cong 0.65$ for the AM controlled flow, at $x/c \cong 0.74$ for the high amplitude sine controlled flow and between x/c=0.45 and x/c=0.28 for the low amplitude sine controlled flow. This similarity in the STFT pattern at the proximity of the separation region, regardless of the mean C_p at which this occurs and to other flow details, such as the presence of low frequency excitation, makes this a proper criteria for the identification of incipient separation. A numerical method is still needed to transform this into a single value.

Fig. 18 shows the RMS of the hot-film data for the above cases. Separation is identified by a sharp rise of the RMS, but this could also be connected to transition. The baseline hot-film RMS slowly rises downstream of separation. This data also indicate that for controlled flows, it is even less appropriate to attempt analyzing the flow using the hot-film RMS. The hot-film RMS values are significantly higher for all of the controlled turbulent boundary layers just downstream of the actuator, and stay virtually constant until $x/c \cong 0.5$

Conclusions

Active separation control in the form of mass-less oscillatory momentum injection was applied for the first time to the slat shoulder of a supercritical airfoil. The slat deflection increased the lifting capability of the airfoil by about 12% and periodic excitation roughly doubled that increment. Low frequency amplitude modulation ($F^+_{AM} \cong 1$) of the high frequency Piezo-actuator was used to save roughly 50% of the excitation momentum required to achieve the same performance gains. Separation was delayed to $x/c \cong 0.7$ with efficient slat shoulder excitation. When AFC is applied to the flap shoulder it is anticipated that the flow will remain attached to the flap as well, allowing increased flap deflection and enhanced lift.

Detailed hot-film, unsteady pressures and PIV data helped in clarifying flow physics issues. A new criteria for separation detection based on short time Fourier transforms of voltage data from a single hot-film sensor was proposed and tested. Future experiments will apply flap separation control on the same airfoil and combinations of flap and slat excitations en route to generating a simplified high lift system.

Acknowledgements

The authors would like to thank the following individuals for their support of the research program, W. L .Sellers, III, M. J. Walsh, A. E. Washburn, L. N. Jenkins, R. D. White, G.C. Hilton, J. Mau, L. M. Hartzheim, I. Fono, S. O. Palmer, R. D. Lewis, and A. R. McGowan.

References

1. Seifert, A. and Pack, L.G., "Oscillatory Control of Separation at High Reynolds Numbers", *AIAA Journal*, Vol. 37, No. 9, 1999 pp. 1062-1071.

2. Seifert, A. and Pack, L.G., "Active Control of Separated Flows on Generic Configurations at High Reynolds Numbers", AIAA Paper 99-3403, June 1999. Accepted by *AIAA Journal*.

3. McClean, J. D., Crouch, J. D., Stoner, R. C., Sakurai, S., Seidel, G. E., Feifel, W. M., and Rush, H. M., 'Study of the Application of Separation Control by Unsteady Excitation to Civil Transport Aircraft", NASA/CR-1999-209338, 1999.

4. Lin J. C. and Dominik, C. J., "Parametric Investigation of a High-Lift Airfoil at High Reynolds Numbers", *Journal of Aircraft*, Vol. 33, No. 4, 1997, pp. 485-491.

5. Lin, J. C., Unpublished EET Data

6. Barlow, J.B., Rae, Jr., W. H., Pope, A., Low Speed Wind Tunnel Testing, 3rd ed. John Wiley and Son, New York, 1999, pp. 328-366.

7. Abbott, I. H., and van Doenhoff, A. E.,"Theory of Wing Sections", Dover Publications, New York, 1949, pp. 227-231.

8. Hoerner, S. F., and Borst, H.V., Fluid-Dynamic Lift: Practical Information on Aerodynamic and Hydrodynamic Lift, Hoerner, Fluid Dynamics, New Jersey, 1975 p. 5-4.

9. Seifert, A., Bachar, T., Koss, D., Shepshelovich, M., and Wygnanski, I., "Oscillatory Blowing, a tool to delay boundary layer separation", *AIAA Journal*, Vol. 31, 1996, pp. 2052-2060

10. Pack, L.G. and Seifert, A.," Dynamics of Active Separation Control at High Reynolds Numbers", AIAA-Paper 2000-0409, January 2000.

11. Amitay, M. and Glezer, A., "Role of actuation frequency in controlled flow reattachment over a stalled airfoil", *AIAA Journal*, Vol. 40, no. 2, Feb. 2002. p. 209-216.

12. Wiltse, J.M., and Glezer, A., "Manipulation of free shear flows using piezoelectric actuators", *Journal of Fluid Mechanics*, Vol. 249, April 1993, pp. 261-285.

13. Margalit, S., Greenblatt, D., Seifert, A., and Wygnanski, I., "Active Control of a Delta Wing at High Incidence using Segmented Piezoelectric Actuators", AIAA Paper 2002-3270, 2002.

14. Bertelrud, A., "Transition on a Three-Element High Lift Configuration at High Reynolds Numbers", AIAA Paper 98-0703, January 1998.

15. Nakayama, A., Stack, J.P., Lin, J. C., "Surface Hot-Film Technique for Measurement of Transition, Separation, and Reattachment Points" AIAA-Paper 93-2918, July 1993.

16. Seifert, A., and Wygnanski, I., "On Turbulent Spots in a Laminar Boundary Layer Subjected to a Self-Similar Adverse Pressure Gradient", *Journal of Fluid Mechanics*, Vol. 296, Aug. 1995, pp. 185-209.

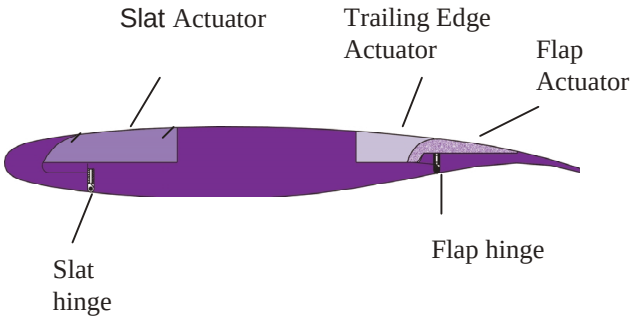

Figure 1a: Modular EET model used for experiment, c=406.4mm

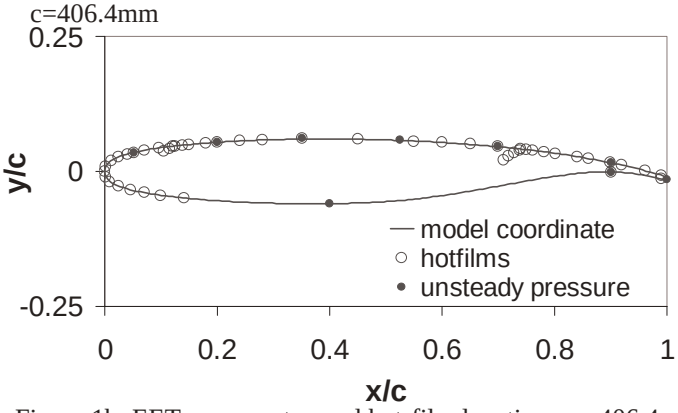

Figure 1b: EET pressure tap and hot-film locations, c=406.4mm. Slat Actuator slots at x/c=0.14 and 0.30.

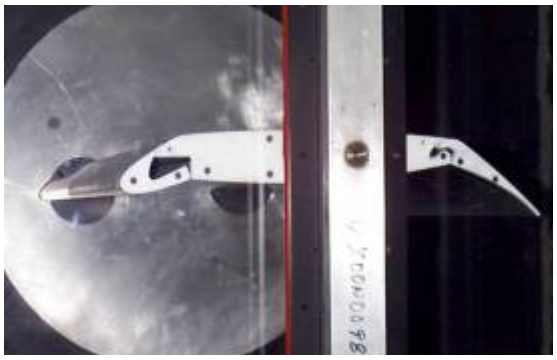

Figure 2: Simplified high lift version of EET airfoil model installed in the BART.

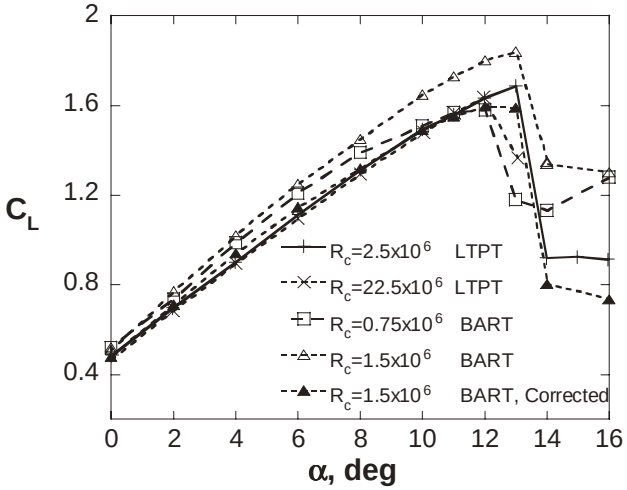

Figure 3a: A comparison of the cruise configuration of the EET airfoil as tested in the BART and LTPT facilities at a range of Reynolds numbers. R_c=0.75x10^6, $\delta_s=\delta_f=0^o$.

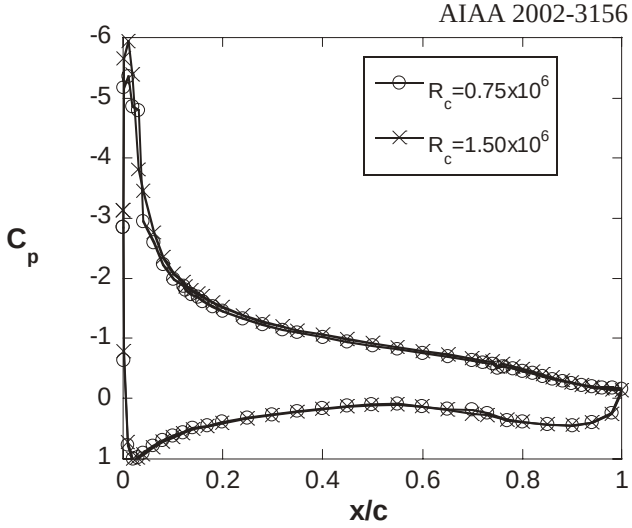

Figure 3b: Airfoil pressure distributions at $\alpha=8^o$ at two Reynolds numbers, $\delta_f=\delta_s=0^o$.

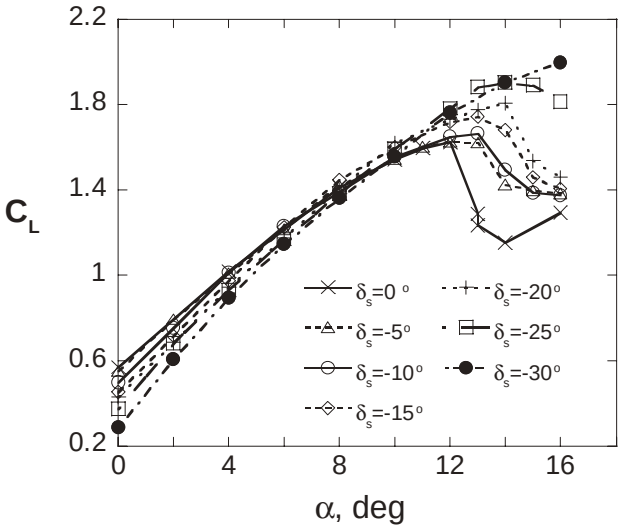

Figure 4: Lift of the EET airfoil at different slat deflections. R_c= 0.75x10^6, $\delta_f=0^o$.

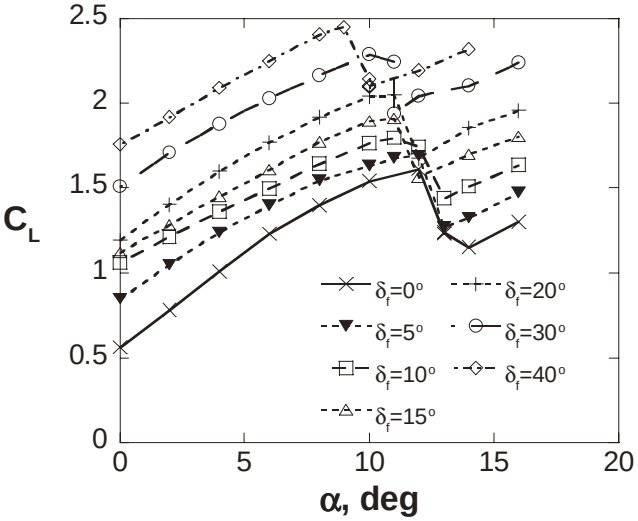

Figure 5a: Lift of the EET airfoil at different flap deflections. R_c= 0.75x10^6, $\delta_s=0^o$.

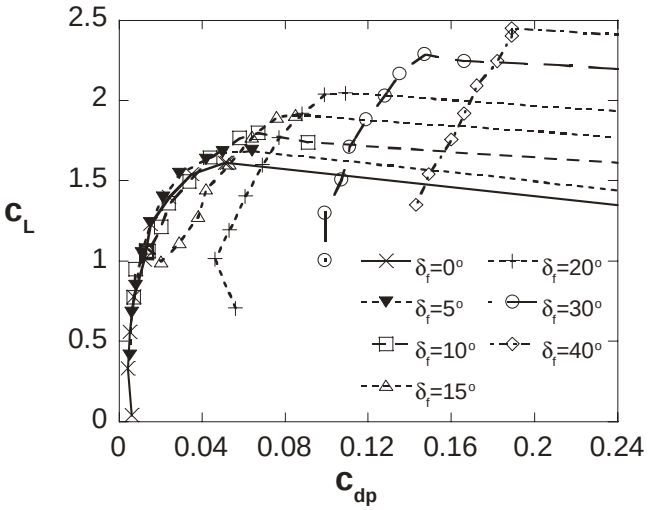

Figure 5b: Lift vs. form drag of the EET airfoil at different flap deflections. R_c= 0.75x10^6, δ_s=0°.

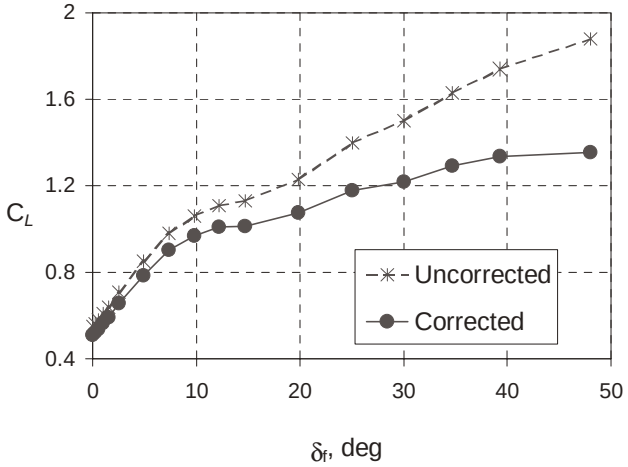

Figure 5c: Corrected and uncorrected lift vs δ_f . R_c=0.75x105, δ_s=0°, α=0°.

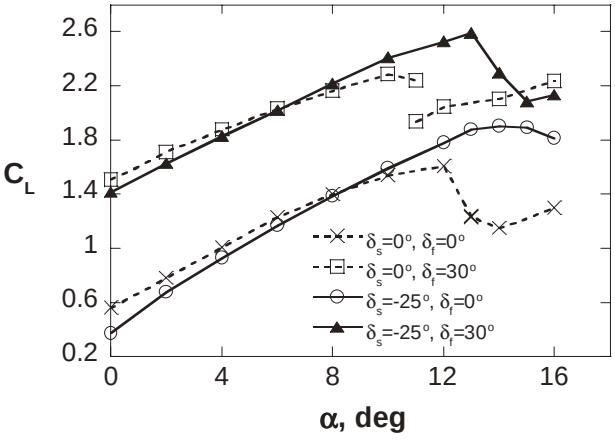

Figure 6: Lift coefficients of the EET airfoil at different high-lift configurations as tested in BART at R_c= 0.75x10^6.

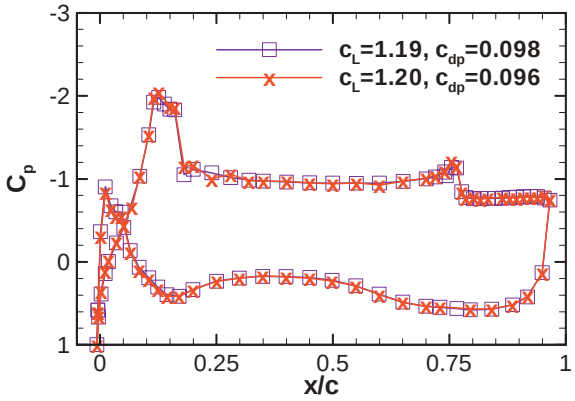

(a) α=-2°

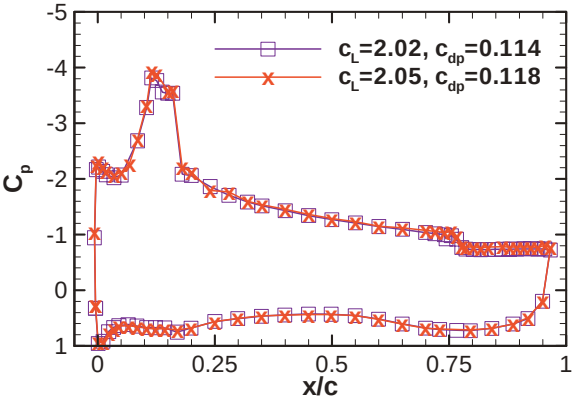

(b) α=6°

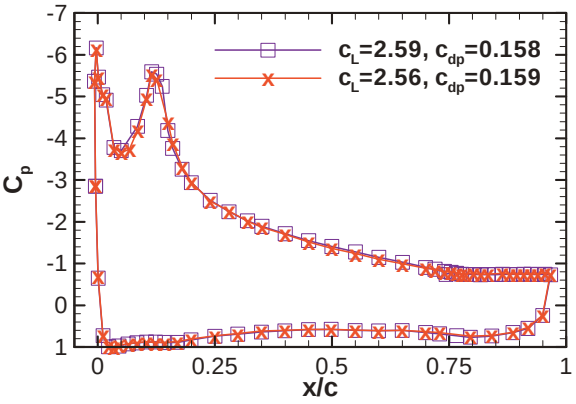

(c) α=13°

Figure 7: Comparison of baseline C_p with and without slots on model. Model with slots is represented by the□. R_c=0.75x10^6, δ_f=30°, δ_s=-25°.

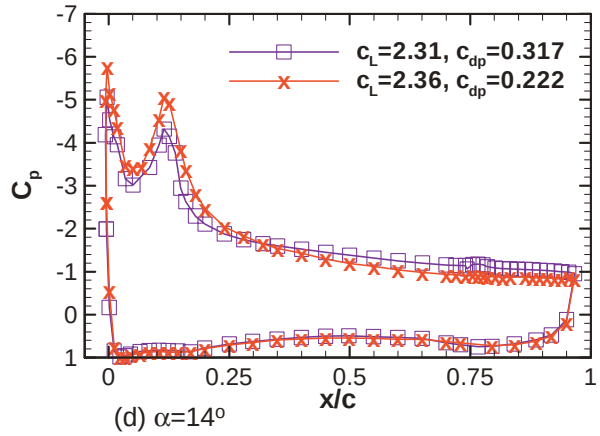

(d) α=14°

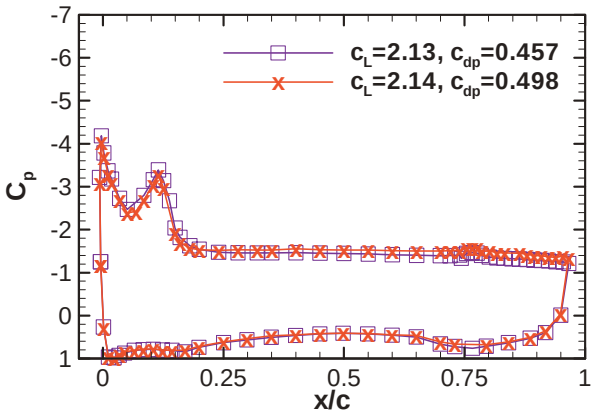

(e) α=15°

Figure 7(d-e): Comparison of baseline C_p with and without slots on model. Model with slots is represented by the□. R_c=0.75x10^6, δ_f=30°, δ_s=-25°.

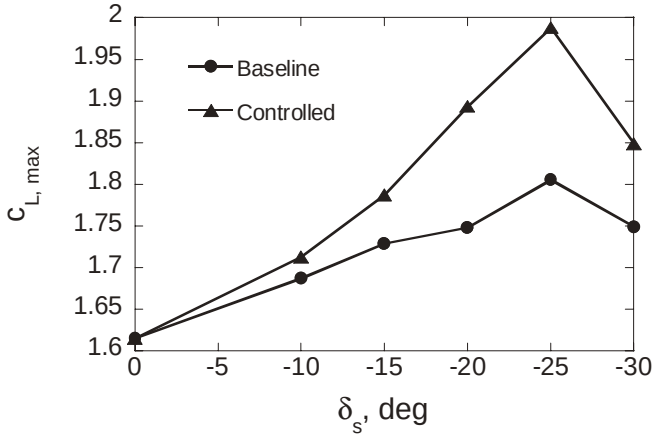

Figure 8 The effect of slat deflection on the baseline and controlled maximum lift coefficient. δ_f=4.3°, R_c=0.75x10^6, both LE actuator slots used, F^+=10.5, C_μ=0.03%.

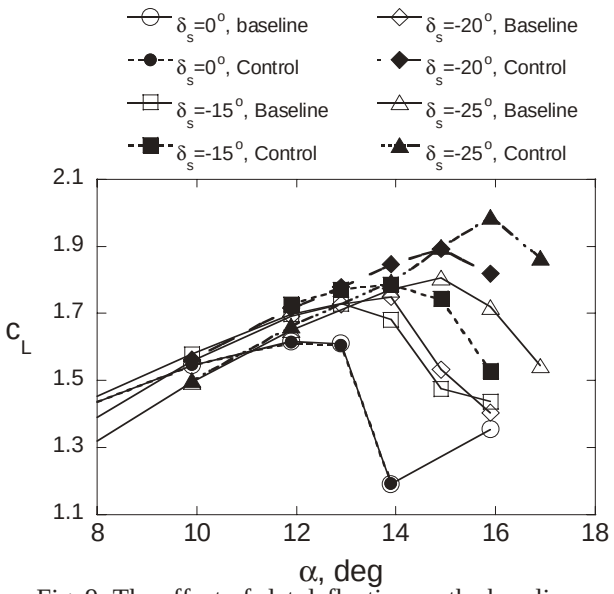

Fig. 9: The effect of slat deflection on the baseline and controlled lift. δ_f=4.3°, R_c=0.75x10^6, both LE actuator slots used, F^+=10.5, $<c_\mu>$=0.03%.

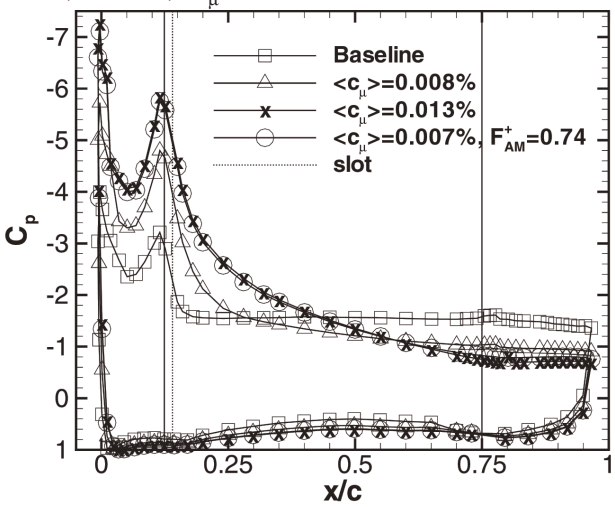

(a) Cp distribution (vertical lines included to indicate flap, slat, and slot locations)

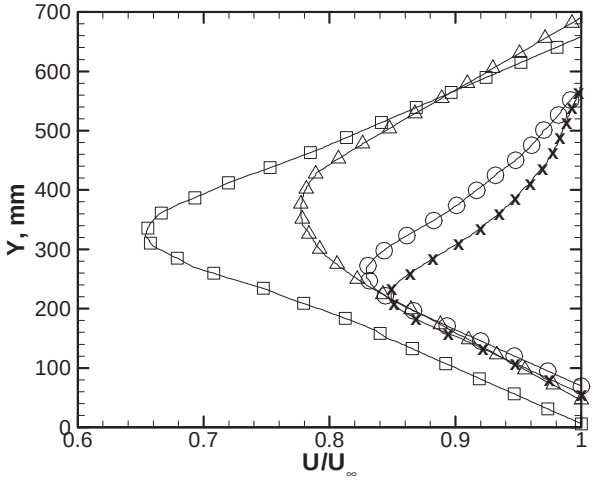

(b) wake distribution.

Figure 10: Efficiency of F^+_{AM}~1 actuation. R_c=0.75x10^6, δ_f=30°, δ_s=-25°, α=15°.

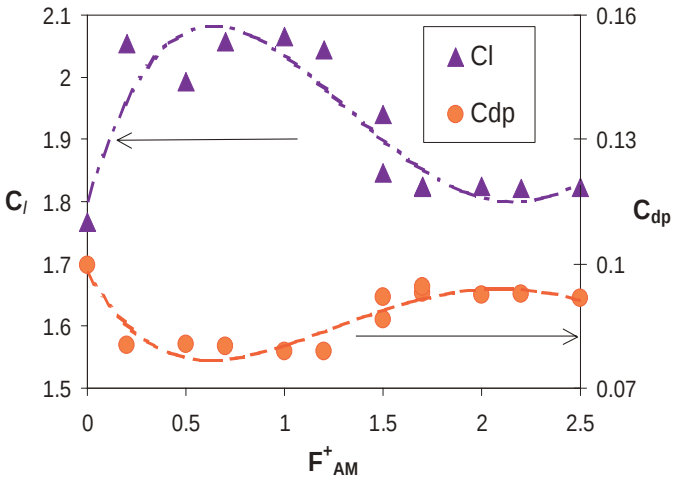

Figure 11: Effect of F^+_{AM} on C_L and C_{dp}.
R_c=0.75x10^6, δ_f=5^o, δ_s=-25^o, $<c_\mu>$=0.003%, α=15^o.

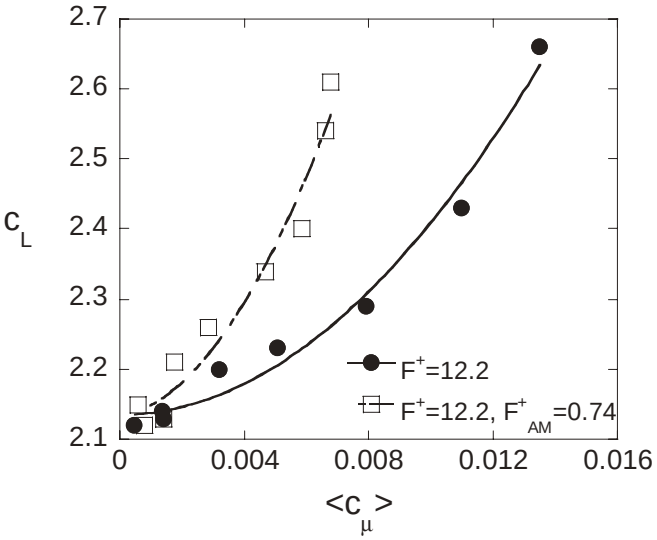

Figure 12 :Comparison of lift due to pure sine wave and AM sine wave, α=15^o, δ_s=-25^o, δ_f=30^o, R_c=0.75x10^6

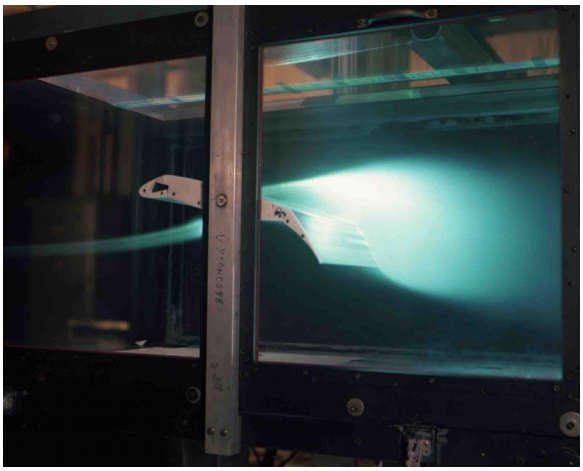

(a) Baseline

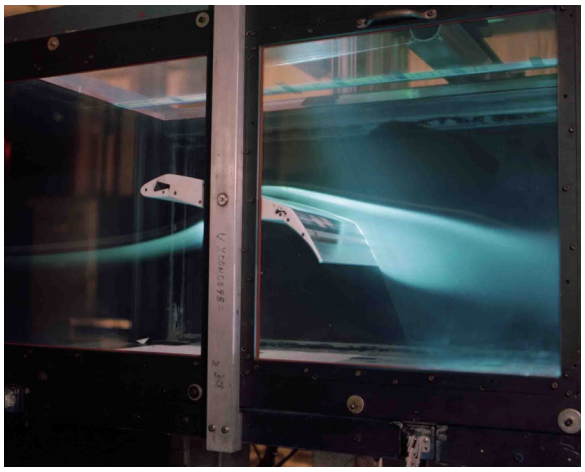

(b) $F^+=12.2$, $\langle c_\mu \rangle=0.013\%$

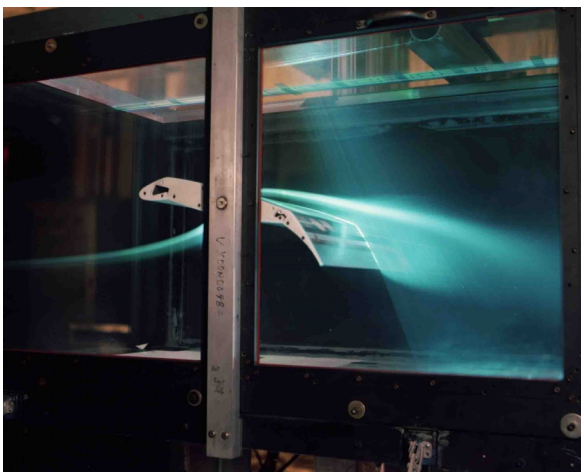

(c) $F^+=12.2$, $F^+_{AM}=0.74$, $\langle c_\mu \rangle=0.007\%$

Figure 13: Flow visualization images with light sheet produced by Argon Ion laser. $\delta_f=30^o$, $\delta_s=-25^o$, $\alpha=15^o$, and $R_c=0.75x10^6$.

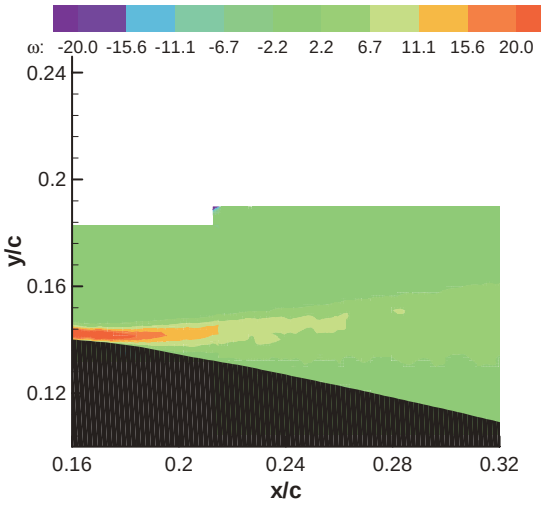

(a) Vorticity contours of baseline flowfield

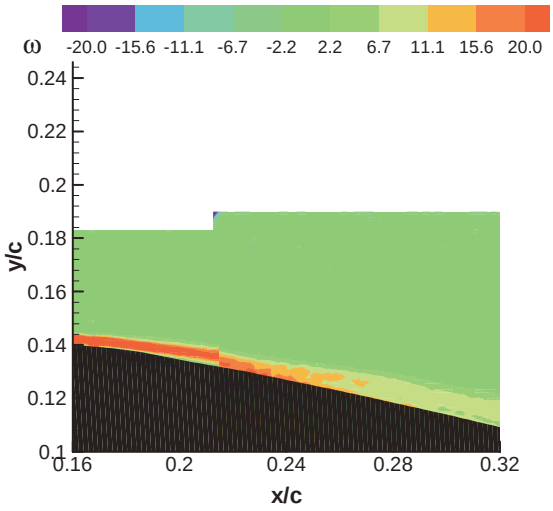

(b) Vorticity contours. $F^+=12.2$, $F^+_{AM}=0.74$, $\langle c_\mu \rangle=0.007\%$

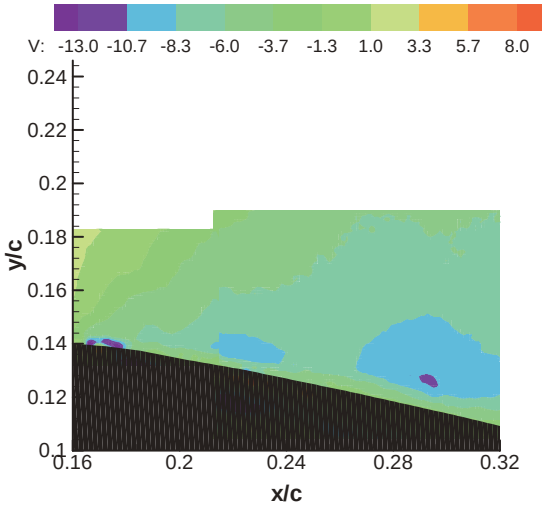

(c) Vertical component of velocity. $F^+=12.2$, $F^+_{AM}=0.74$, $\langle c_\mu \rangle=0.007\%$

Fig. 14: PIV data, $\delta_f=30^o$, $\delta_s=-25^o$, $\alpha=15^o$. Slot at x/c=0.163 in coordinate system shown.

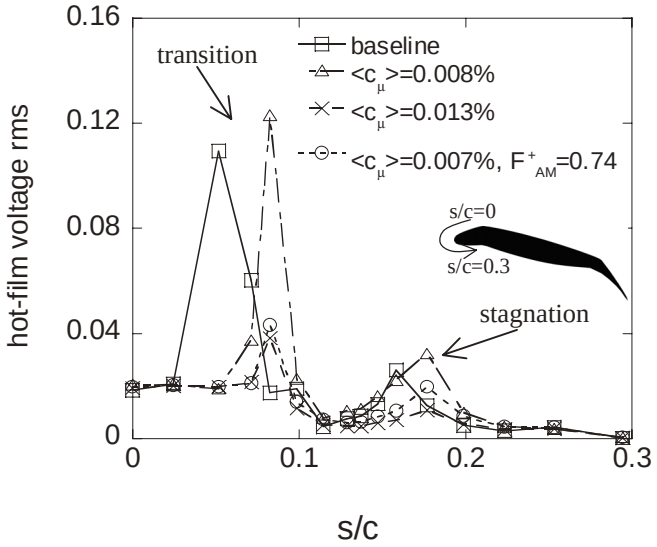

Figure 15: Slat hot-film voltage RMS, δ_f=30º, δ_s=-25º, α=15º, R_c=0.75x10$^{6.}$ s/c=0 is at x/c=0.085 on upper surface. F^+=12.2 when control applied.

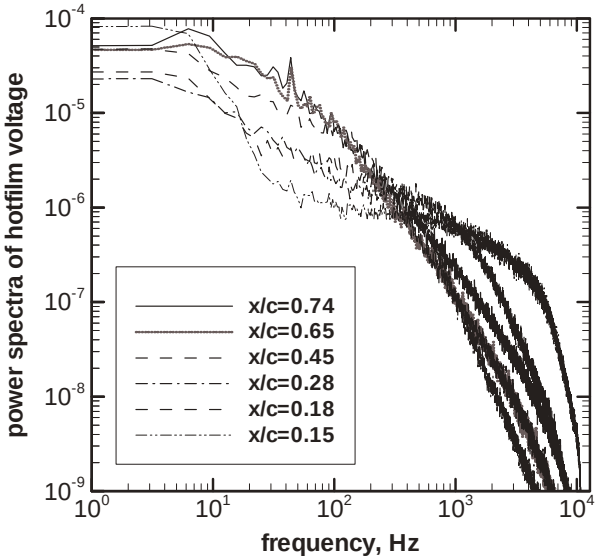

Figure 16: Main element hot-film voltage spectra of baseline model. δ_f=30, δ_s=-25º, α=15º, R_c=0.75x10$^{6.}$

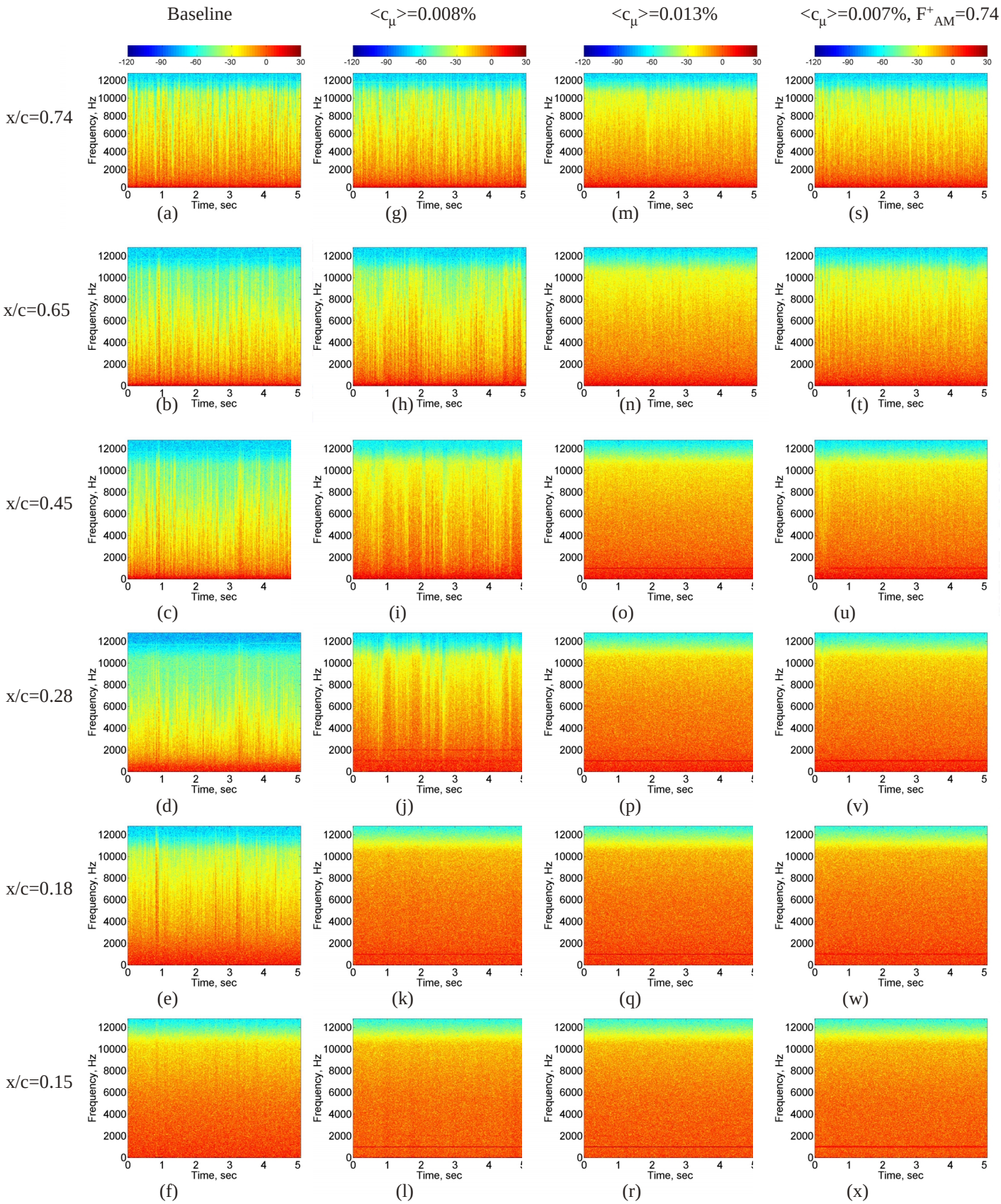

Figure17: STFT of hot-film voltages on airfoil main element at R_c=0.75x10^6, δ_f=30^o, δ_s=-25^o. F^+=12.2 when control applied. F^+=12.2 modulated at F^+_{AM}=0.74 for right hand side column (s-x).

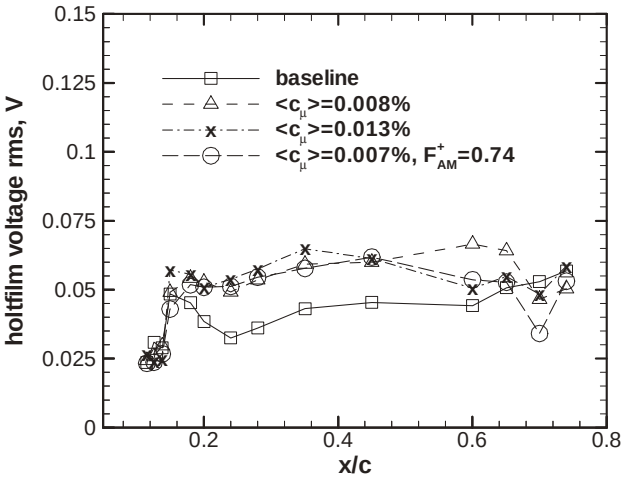

Figure18: Main element hot-film voltage RMS values for conditions of Figure 10a.